Materials Science in Semiconductor Processing 27 (2014) 854–859

Contents lists available at ScienceDirect

Materials Science in Semiconductor Processing

journal homepage: www.elsevier.com/locate/mssp

Synthesis and magnetic properties of $ZnFe_{1.97}RE_{0.03}O_4$ (RE = Eu and Nd) nanoparticles

Shuo Yang [a,b], Donglai Han [a,b], Zhe Wang [c], Yang Liu [c], Gang Chen [c], Hongmei Luan [c], Bayanheshig [a], Lili Yang [c,*]

[a] Changchun Institute of Optics Fine Mechanics and Physics, Chinese Academy of Sciences, Changchun 130033, China
[b] University of Chinese Academy of Sciences, Beijing 100049, China
[c] Key Laboratory of Physics and Chemistry of Functional Materials (Ministry of Education), Jilin Normal University, Changchun 130103, China

ARTICLE INFO

Available online 17 September 2014

Keywords:
Zinc ferrite
Paramagnetism
Ferromagnetism

ABSTRACT

The $ZnFe_{1.97}RE_{0.03}O_4$ (RE = Eu and Nd) nanoparticles (NPs) were prepared via the sol–gel method. We investigated the effect of RE^{3+} doping on the spinel structure and the magnetic properties of the samples. Compared to the paramagnetism of pure $ZnFe_2O_4$, the $ZnFe_{1.97}Eu_{0.03}O_4$ and $ZnFe_{1.97}Nd_{0.03}O_4$ NPs exhibit weak ferromagnetic properties, since the formation of defects in $ZnFe_2O_4$ caused by RE^{3+} doping not only create energy levels within the band gap to hybridize with the 4f levels RE^{3+} and trigger the onset of magnetic order, but also work as the pinning centers to impede the rotation of the magnetization and give rise to the enhanced coercivity. Moreover, the coercivity and saturation magnetization of $ZnFe_{1.97}Nd_{0.03}O_4$ NPs are stronger than those of $ZnFe_{1.97}Eu_{0.03}O_4$ NPs due to the larger spin and orbital moments of Nd^{3+} ions.

1. Introduction

As an important member of ferrite family, zinc ferrite ($ZnFe_2O_4$) has attracted significant research interest due to their unique structural and magnetic properties. $ZnFe_2O_4$ is a chemically and thermally stable semiconductor material, which is suitable for wide applications including photocatalyst, gas sensor, magnetic data storage, ferrofluid, magnetic resonance imaging, drug delivery, pigment, and hot-gas desulfurization [1–6].

For improving their performance in different applications, people usually try to dope different transition metal (TM) elements, such as, Mn, Co, Ni and so on, into the ferrite lattices and further vary their amounts to obtain the desired magnetic and dielectrical properties of ferrites [7–10]. In stead of the above transition metals, the rare earths is another desirable choice for tuning the physical properties of ferrites, not only because the lanthanide contraction can induce the monotonic change of ionic radii, but also because the sequential filling of electrons in their 4f shells brings the different stable oxidation states and the periodical variation in magnetic moments. So far, the RE ions are usually introduced into the TM-doped $ZnFe_2O_4$ spinel ferrites [11–13]. Few works have been reported about the RE-doped $ZnFe_2O_4$ ferrites. Since the pure $ZnFe_2O_4$ usually exhibits paramagnetic properties at room temperature, the introduction of RE ions may bring interesting magnetic properties, which is necessary to be investigated.

In this paper, we selected Eu and Nd elements to dope $ZnFe_2O_4$ nanoparticles with sol–gel method. The doping effects on their structural and magnetic properties were investigated in detail.

* Corresponding author.
E-mail address: llyang@jlnu.edu.cn (L. Yang).

http://dx.doi.org/10.1016/j.mssp.2014.08.032
1369-8001/

2. Experimental

2.1. Synthesis

RE (RE=Eu and Nd) doped $ZnFe_2O_4$ nanoparticles were synthesized via the sol–gel method. For $ZnFe_{1.97}RE_{0.03}O_4$ nanoparticles, the citric acid (CA), Zn $(NO_3)_2 \cdot 6H_2O$ and Fe $(NO_3)_3.9H_2O$ were firstly dissolved in 200 ml deionized water with a molar ratio of 3: 1: 2. The Eu_2O_3 powder was dissolved in 0.1 mol/L nitric acid aqueous solution to form europium nitrate. Then the europium nitrate was added into the above mixture with a Zn: Eu molar ratio of 1:0.03. Likewise, neodymium nitrate was added into the above mixture with a Zn: Nd molar ratio of 1:0.03. The two mixtures were then magnetic stirred for 24 h at the room temperature, respectively. After stirring, the two solutions were kept in a dry cabinet at 80 °C for 48 h to obtain $ZnFe_{1.97}Eu_{0.03}O_4$ and $ZnFe_{1.97}Nd_{0.03}O_4$ gel. After that, we adjusted the dry cabinet to 120 °C for puffing 24 h to obtain the xerogels. Herein, we obtained the precursors. These two precursor powders were annealed at 750 °C in air for 2 h to get the final samples. For comparison, we also prepared pure $ZnFe_2O_4$ sample in the similar process only without adding Eu^{3+} and Nd^{3+} solution.

2.2. Characterization

X-ray diffraction (XRD) patterns were recorded by a MAC Science MXP-18 X-ray diffractometer using a Cu target radiation source was used to study the crystal structure and morphology of the samples. The scanning electron microscope (SEM, S-570, Hitachi) with an energy dispersive spectrometer (EDS) was used to characterize the morphology and different chemical compositions of the samples. The transmission electron microscope (TEM, JEM-2100, JEOL) spectroscopy system was used to qualitatively confirm the detailed microscopic structure. A quantitative compositional analysis was carried out by using an X-ray photoelectron spectroscopy (XPS) in an ultra-high vacuum chamber at a pressure lower than 1.333×10^{-7} Pa. The magnetic properties of the samples were measured by a Lake Shore 7407 vibrating sample magnetometry (VSM).

3. Results and discussion

The XRD patterns of $ZnFe_2O_4$, $ZnFe_{1.97}Eu_{0.03}O_4$, $ZnFe_{1.97}Nd_{0.03}O_4$ NPs are shown in Fig. 1. For all XRD patterns, the diffraction peak position and relative intensity match well with the standard patterns of $ZnFe_2O_4$ (JCPDS file No. 22-1012), which was indexed in the spinel-like structure. For $ZnFe_2O_4$ NPs, the diffraction peaks at 2θ values of 29.8°, 35.09°, 42.71°, 56.5°, and 62.04° could be ascribed to the reflection of (220), (311), (400), (511) and (440) planes respectively. For the XRD patterns of $ZnFe_{1.97}Eu_{0.03}O_4$, $ZnFe_{1.97}Nd_{0.03}O_4$ NPs, no diffraction peaks are detected from europium oxides and neodymium oxides, which indicates the Eu^{3+} and Nd^{3+} ions successfully incorporated into $ZnFe_2O_4$ matrix. Compare to the pure $ZnFe_2O_4$, the diffraction peak positions of $ZnFe_{1.97}Eu_{0.03}O_4$ and $ZnFe_{1.97}Nd_{0.03}O_4$ NPs shift to lower angle, and the diffraction peak positions of $ZnFe_{1.97}Nd_{0.03}O_4$ NPs

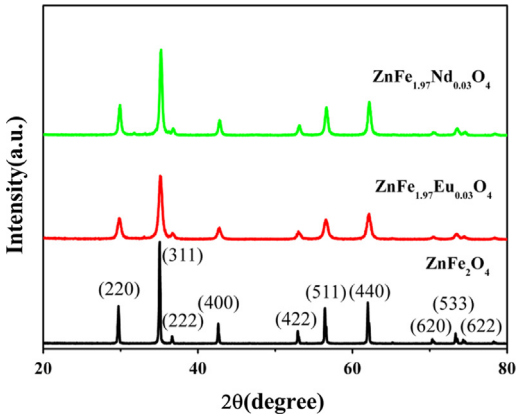

Fig. 1. XRD patterns of $ZnFe_2O_4$, $ZnFe_{1.97}Eu_{0.03}O_4$, $ZnFe_{1.97}Nd_{0.03}O_4$ NPs.

shift more, which is mainly due to that ionic radius of Nd^{3+} (0.116 nm) and Eu^{3+} (0.107 nm) is higher than Zn^{2+}(0.074 nm) and Fe^{3+} (0.065 nm). We also find in Fig. 1 that the full width at half-maximum (FWHM) of $ZnFe_{1.97}Eu_{0.03}O_4$ and $ZnFe_{1.97}Nd_{0.03}O_4$ NPs turn broader in comparison with that of $ZnFe_2O_4$ NPs, indicating the degeneration of crystalline qualities. Moreover, the broader FWHM is also related to the decrease of crystalline size of samples. To prove that, we calculate the average crystalline size of three samples using the Scherer equation

$$D = \frac{0.89\lambda}{\beta \cos \theta} \quad (1)$$

where D is the crystalline size, λ is the wavelength of the X-ray radiation, θ is Bragg's angle, and β is the FWHM on 2θ scale. According to Eq. (1), the calculated average crystalline size of $ZnFe_2O_4$, $ZnFe_{1.97}Eu_{0.03}O_4$ and $ZnFe_{1.97}Nd_{0.03}O_4$ NPs is 42.32 nm, 17.82 nm and 14.69 nm, respectively. Clearly, with doping Eu^{3+} and Nd^{3+}, the size of the samples decreased, indicating the incorporation of Eu^{3+} and Nd^{3+} into $ZnFe_2O_4$ restrained the lattice growth. The bigger ionic radius of dopant has, the stronger restraint effect happens.

To clearly see the morphology of $ZnFe_{1.97}Eu_{0.03}O_4$ and $ZnFe_{1.97}Nd_{0.03}O_4$ NPs, we present their SEM images in Fig. 2. As shown in Fig. 2a and c, we can see that most of the NPs have been aggregated together to form some big rocks with some small particles adsorbed on their surfaces. We further perform the energy-dispersive spectrum (EDS) measurement on these samples to verify the chemical composition, which are shown in Fig. 2b and d. We can find that, except the Zn, Fe and O elements, a small amount of Eu and Nd elements exist in $ZnFe_{1.97}Eu_{0.03}O_4$ and $ZnFe_{1.97}Nd_{0.03}O_4$ NPs, respectively. The corresponding quantitative concentration is 2.69% and 2.28% for Eu and Nd elements, respectively, which is close to their expected doping concentration.

To reveal their detailed microscopic structure, we use TEM technique to characterize the $ZnFe_{1.97}Eu_{0.03}O_4$ and $ZnFe_{1.97}Nd_{0.03}O_4$ NPs. From Fig. 3a, we can see that the average size of $ZnFe_{1.97}Eu_{0.03}O_4$ NPs is ~20 nm. As shown in Fig. 3b, the average size of $ZnFe_{1.97}Nd_{0.03}O_4$

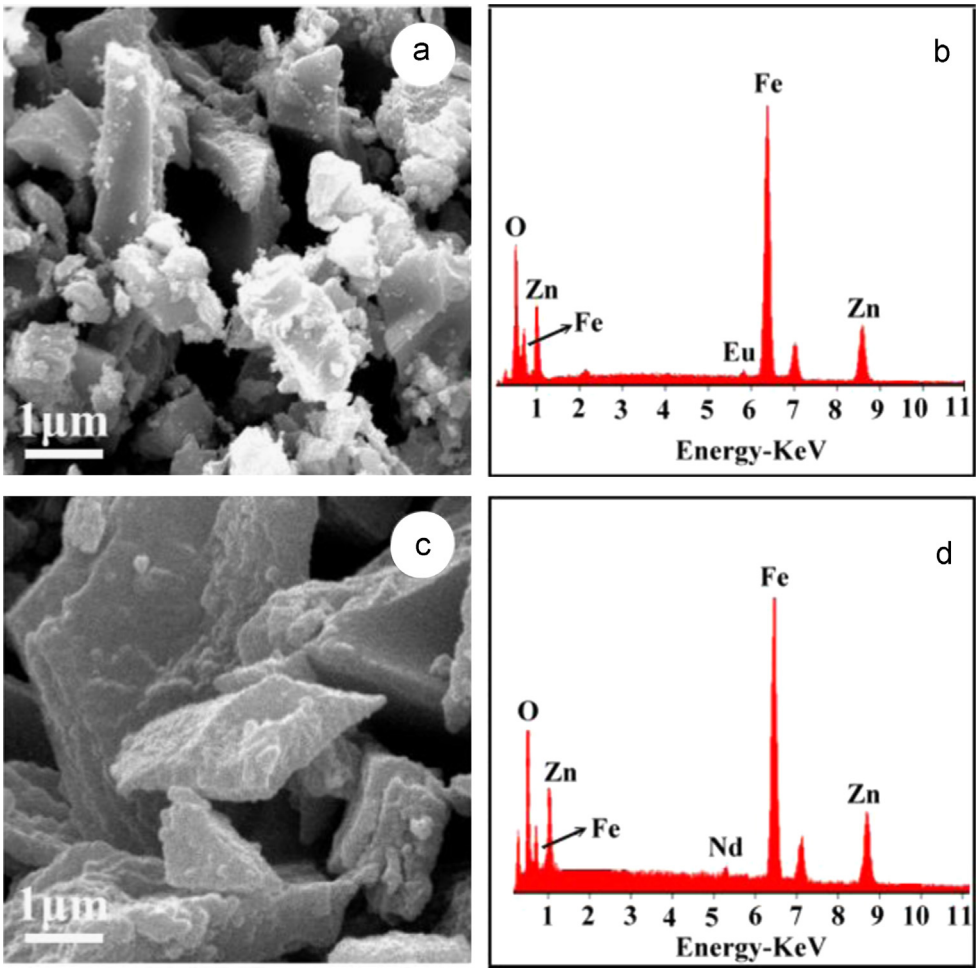

Fig. 2. SEM and EDS images of $ZnFe_{1.97}Eu_{0.03}O_4$, $ZnFe_{1.97}Nd_{0.03}O_4$ NPs.

NPs is ~15 nm. Normally, the size of $ZnFe_{1.97}Nd_{0.03}O_4$ should be larger than that of $ZnFe_{1.97}Eu_{0.03}O_4$ since the ionic radius of Nd^{3+} (0.116 nm) is bigger than that of Eu^{3+} (0.107 nm). While, in our case, the size of $ZnFe_{1.97}Nd_{0.03}O_4$ NPs is smaller than that of $ZnFe_{1.97}Eu_{0.03}O_4$ NPs, which maybe due to relatively lower doping concentration of Nd according to the EDS results. Moreover, the HRTEM images of two samples have been presented in Fig. 3b and d. The fringe space is determined to be 0.315 nm and 0.322 nm corresponding to (220) plane distance of the standard spinel structure for $ZnFe_{1.97}Eu_{0.03}O_4$ and $ZnFe_{1.97}Nd_{0.03}O_4$ NPs, respectively. We can see that this fringe space in our case is bigger than that of standard $ZnFe_2O_4$ (0.298 nm), which is mainly caused by the cell volume expansion with Eu^{3+} and Nd^{3+} doping into $ZnFe_2O_4$ lattices since their ionic radius is much bigger than that of Fe^{3+} and Zn^{2+}.

To further investigate the chemical compositions and bonding states, we perform XPS measurements on the $ZnFe_{1.97}Eu_{0.03}O_4$ and $ZnFe_{1.97}Nd_{0.03}O_4$ NPs. Prior to the XPS measurements, the samples were cleaned by sputtering with an Ar ion beam to remove any potential surface contamination. The Zn 2p XPS spectra of $ZnFe_{1.97}Eu_{0.03}O_4$ and $ZnFe_{1.97}Nd_{0.03}O_4$ NPs are shown in Fig. 4a. We can find two peaks located at 1021.1 eV and 1044.1 eV, which corresponds to the Zn $2p_{3/2}$ and Zn $2p_{1/2}$ core lines, respectively. Fig. 4b presents the O1s XPS spectra of $ZnFe_{1.97}Eu_{0.03}O_4$ and $ZnFe_{1.97}Nd_{0.03}O_4$ NPs. The deconvolutions show the presence of two different oxygen species in both samples. The binding energy peak located at 529.6 eV is associated with the lattice oxygen, while the binding energy peak located at 531.6 eV is corresponding to the non-lattice oxygen (included adsorbed oxygen and oxygen in amorphous $ZnFe_2O_4$) [14,15]. Fig. 4c presented the Eu3d XPS spectrum of $ZnFe_{1.97}Eu_{0.03}O_4$ NPs. The two characteristic peaks at 1163.6 and 1134.5 eV can be assigned to the core levels of Eu $3d_{3/2}$ and Eu $3d_{5/2}$, respectively. It indicates the Eu ions appear with trivalence. Fig. 4d depicted the Nd 3d XPS spectrum. The two characteristic peaks at 982.3 eV and 1005.3 eV can be assigned to the core levels of Nd $3d_{5/2}$ and Eu $3d_{3/2}$, respectively, which reveals that Nd ions existed in trivalent state [16–19]. Therefore, according to both XRD and XPS results, we can deduce that Eu^{3+} and Nd^{3+} ions have successfully incorporated into $ZnFe_2O_4$ lattices and substituted for the sites of Fe ions.

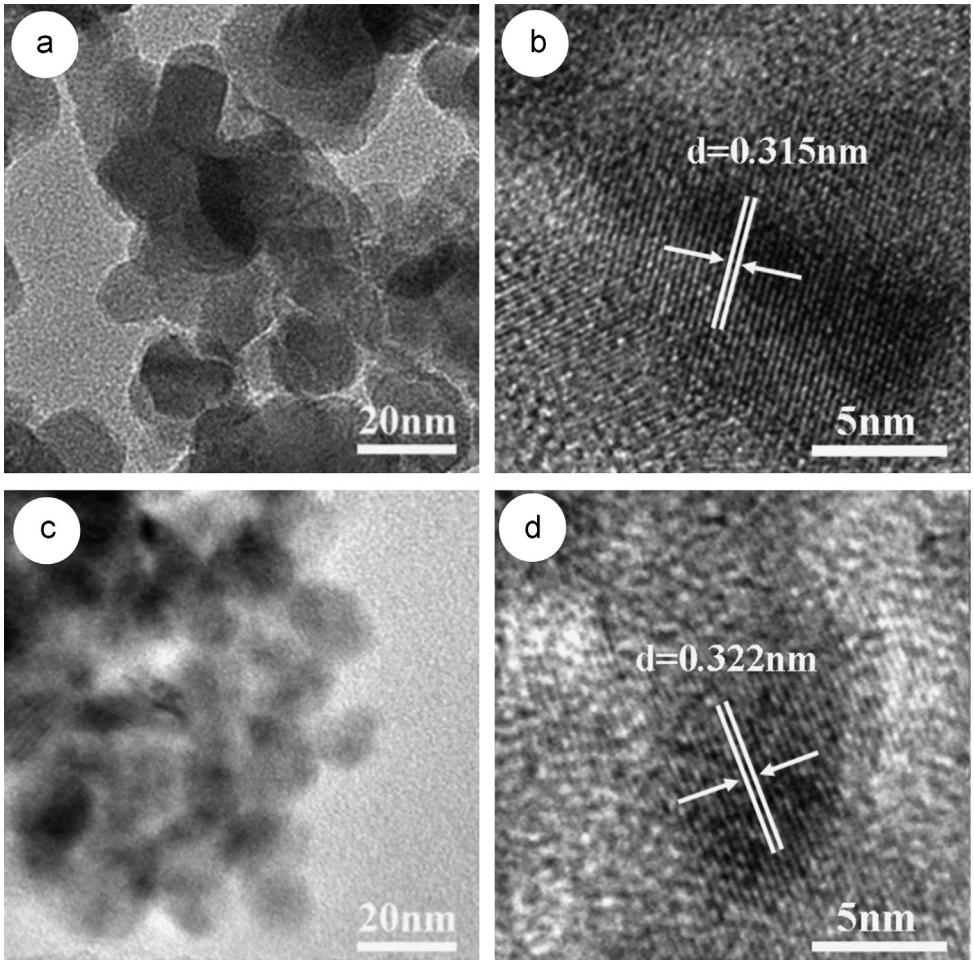

Fig. 3. TEM and HRTEM images of $ZnFe_{1.97}Eu_{0.03}O_4$, $ZnFe_{1.97}Nd_{0.03}O_4$ NPs.

The magnetic properties are the most important properties for ferrites, which are depending on the processing conditions, microstructure, chemical composition and the type of the additives [20,21]. Fig. 5 shows the hysteresis loops for $ZnFe_2O_4$, $ZnFe_{1.97}Eu_{0.03}O_4$ and $ZnFe_{1.97}Nd_{0.03}O_4$ NPs. For the hysteresis loop of pure $ZnFe_2O_4$ NPs, at low field, the patterns depict hysteresis with finite coercivity and a tendency of saturation whereas at high field the magnetization tends to increase almost linearly, reflecting a paramagnetic behavior. This shows that the $ZnFe_2O_4$ is normal spinel, with Zn^{2+} in tetrahedral sites and Fe^{3+} in octahedral sites with antiparallel arrangement of magnetic moments [22]. However, the $ZnFe_{1.97}Eu_{0.03}O_4$ and $ZnFe_{1.97}Nd_{0.03}O_4$ NPs exhibit the weak ferromagnetic behavior. Due to the different number of intra-4f shells, Eu^{3+} and Nd^{3+} could lead to the local lattice distortion and lower the formation energy of defects in $ZnFe_2O_4$. These defects created energy levels within the band gap, which presumably hybridized with the 4f levels of RE^{3+} and triggered the onset of magnetic order. These defects also worked as the pinning centers to impede the rotation of the magnetization [19,23], giving rise to the enhanced coercivity. Moreover, the values of saturation magnetization M_s and coercivity H_c were 10 memu/g and 17.3 Oe for $ZnFe_{1.97}Eu_{0.03}O_4$ NPs, 15 memu/g and 143.5 Oe for $ZnFe_{1.97}Nd_{0.03}O_4$ NPs, respectively. Obviously, M_s and H_c of $ZnFe_{1.97}Nd_{0.03}O_4$ NPs are stronger than those of $ZnFe_{1.97}Eu_{0.03}O_4$ NPs, which also can be seen from the inset of Fig. 5. Different from Eu^{3+}, Nd^{3+} owns larger spin and orbital moments, which could contribute to the magnetism if the crystal field does not quench the orbital moment. It was not surprising that the $ZnFe_{1.97}Nd_{0.03}O_4$ NPs acquire giant magnetocrystalline anisotropy energy if the anisotropic orbital moments of Nd ions were taken into account, the orbital moment would make a significant contribution to the magnetic ordering with giant anisotropy [24,25].

4. Conclusions

We prepared $ZnFe_{1.97}RE_{0.03}O_4$ (RE=Eu and Nd) NPs via the sol–gel method and investigated the effect of RE^{3+} doping on the spinel structure and their magnetic properties. Compare to the paramagnetism of pure $ZnFe_2O_4$, the $ZnFe_{1.97}Eu_{0.03}O_4$ and $ZnFe_{1.97}Nd_{0.03}O_4$ NPs exhibit weak ferromagnetic properties, since the formation of defects in $ZnFe_2O_4$ caused by RE^{3+} doping not only create energy levels within the band gap to hybridize with the 4f levels RE^{3+} and trigger the onset of magnetic order, but also

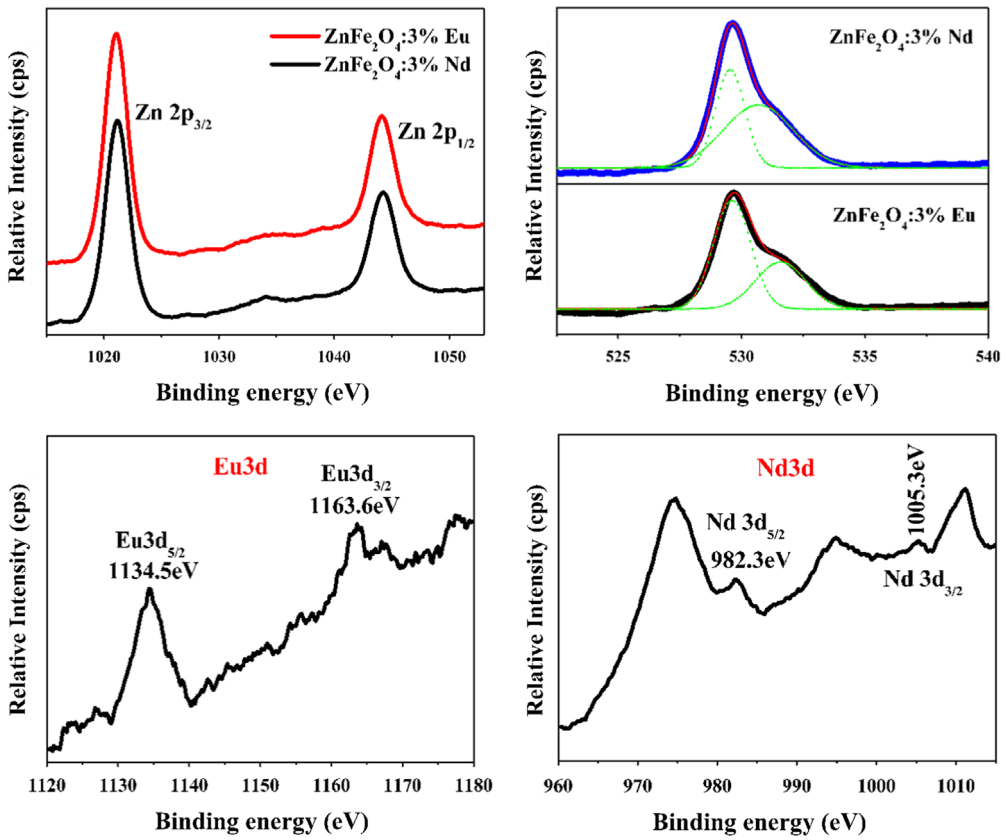

Fig. 4. XPS spectrum of RE (RE=Eu and Nd) doped $ZnFe_2O_4$ nanoparticles. (a) Zn $2p_{3/2}$ and Zn $2p_{1/2}$ XPS spectrum; (b) O1s XPS spectrum where two components (green curves) were used to deconvolute the experimental peak; (c) Eu $3d_{5/2}$ and Eu $3d_{3/2}$ XPS spectrum; (d) Nd $3d_{5/2}$ and Nd $3d_{3/2}$ XPS spectrum. (For interpretation of the references to color in this figure legend, the reader is referred to the web version of this article.)

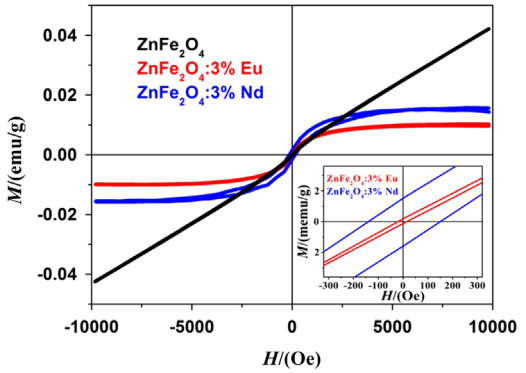

Fig. 5. Hysteresis loops of $ZnFe_2O_4$, $ZnFe_{1.97}Eu_{0.03}O_4$ and $ZnFe_{1.97}Nd_{0.03}O_4$ NPs. The inset shows the magnification of the curve near coercivity region.

work as the pinning centers to impede the rotation of the magnetization and give rise to the enhanced coercivity. Moreover, the ferromagnetism of $ZnFe_{1.97}Nd_{0.03}O_4$ NPs is stronger than that of $ZnFe_{1.97}Eu_{0.03}O_4$ NPs. Moreover, the coercivity and saturation magnetization of $ZnFe_{1.97}Nd_{0.03}O_4$ NPs are stronger than those of $ZnFe_{1.97}Eu_{0.03}O_4$ NPs due to the larger spin and orbital moments of Nd^{3+} ions. Our results not only provide a candidate material for magnetocaloric applications, but inspire people to deeply investigate the rare-earth doped $ZnFe_2O_4$ nanoparticles in both theoretical and experimental aspects.

Acknowledgments

The authors would like to acknowledge financial support for this work from National Nature Science Foundation of China (Grant nos. 11204104, 61178074, 61008051 and 11254001), Program for the Development of Science and Technology of Jilin province (Item nos. 20110415, 201115219 and 20100113), program for the Master Students' Scientific and Innovative Research of Jilin Normal University (Item nos. 201112, 201101 and 201139).

References

[1] P. Kinnari, R.V. Upadhyay, R.V. Mehta, J. Magn. Magn. Mater. 252 (2002) 35.
[2] M.H. Sousa, F.A. Tourinho, J. Depeyrot, G. Josa da Silva, M.C.F.L. Lara, J. Phys. Chem. B 105 (2001) 1168.
[3] S. Chander, S. Kumar, A. Krishnamurthy, B.K. Srivastava, V.K. Aswal, Pramana, J. Phys. 61 (2003) 617.
[4] S. Nakashima, K. Fujita, K. Tanaka, K. Hirao, J. Phys.: Condens. Matter 17 (2005) 137.
[5] T. Pannaparayil, S. Komarneni, R. Marande, M. Zadarko, J. Appl. Phys. 67 (1990) 5509.

[6] G.F. Goya, H.R. Rechenberg, M. Chen, W.B. Yelon, J. Appl. Phys. 87 (2000) 8005.
[7] C.N. Chinnasamy, A. Narayanasamy, N. Ponpandian, K. Chattopadhyay, H. Guerault, J.-M. Greneche, J. Phys.: Condens. Matter 12 (2000) 7795.
[8] V. Sepelak, S. WiBmann, K.D. Becker, J. Magn. Magn. Mater. 203 (1999) 135.
[9] F. Grasset, N. Labhsetwar, D. Li, D.C. Park, N. Saito, H. Haneda, O. Cador, T. Roisnel, S. Mornet, E. Duguet, J. Portier, J. Etourneau, Langmuir 18 (2002) 8209–8216.
[10] Y. Ahn, E.J. Choi, S. Kim, D.H. An, K.U. Kang, B.-G. Lee, K.S. Baek, H.N. Oak, J. Korean Phys. Soc. 41 (2002) 123–128.
[11] A.C.F.M. Costa, E. Tortella, M.R. Morelli, R.H.G.A. Kiminami, Synthesis, micro- structure and magnetic properties of Ni–Zn ferrites, J. Magn. Magn. Mater. 256 (2003) 174–182.
[12] Y.P. Fu, C.H. Lin, Microwave-induced combustion synthesis of Ni–Zn ferrite powder and its characterization, J. Magn. Magn. Mater. 251 (2002) 74–79.
[13] J.H. Lee, C.K. Kim, S. Katoh, R. Murakami, Microwave-hydrothermal versus conventional hydrothermal preparation of Ni- and Zn-ferrite powders, J. Alloys Compd. 325 (2001) 276–280.
[14] A.B. Djurisic, Y.H. Leung, K.H. Tam, Y.F. Hsu, L. Ding, W.K. Ge, Y.C. Zhong, K.S. Wong, W.K. Chan, H.L. Tam, K.W. Cheah, W. M. Kwok, D.L. Phillips, Defect emissions in ZnO nanostructures, Nanotechnology 18 (2007) 095702–095709.
[15] F. Jamali-Sheini, R. Yousefi, K.R. Patil, Surface characterization of Au–ZnO nanowire films, Ceram. Int. 38 (2012) 6665–6670.
[16] L. Armelao, G. Bottaro, M. Pascolini, M. Sessolo, E. Tondello, M. Bettinelli, A. Speghini, J. Phys. Chem. C 112 (2008) 4049.
[17] R.H. Shin, J.H. Lee, G. Kim, W. Jo, D.H. Kim, H.J. Lee, J. Kang, Jpn. J. Appl. Phys. 49 (2010) 09150115.
[18] Z.H. Zhang, X.L. Zhong, H. Liao, F. Wang, J.B. Wang, Y.C. Zhou, Appl. Surf. Sci. 257 (2011) 7461.
[19] Dandan Wang, Qian Chen, Guozhong Xing, Jiabao Yi, Saidur Rahman Bakaul, Jun Ding, Jinlan Wang, Tom Wu, Nano Lett. 12 (2012) 3994–4000.
[20] K. Kondo, T. Chiba, S. Yamada, Effect of microstructure on magnetic properties of Ni–Zn femtes, J. Magn. Magn. Mater. 541 (2003) 254–255.
[21] A.C.F.M. Costa, E. Tortella, M.R. Morelli, R.H.G.A. Kiminami, Synthesis, microstructure and magnetic properties of Ni–Zn femtes, J. Magn. Magn. Mater. 256 (2003) 174.
[22] S. Ayyappan, S. Philip Raja, C. Venkateswaran, J. Philip, B. Raj, Appl. Phys. Lett. 96 (2010) 143106.
[23] J.D. Livingston, J. Appl. Phys 52 (1981) 2544.
[24] P. Bruno, Phys. Rev. B 39 (1989) 865.
[25] G.H.O. Daalderop, P.J. Kelly, M.F.H Schuurmans, Phys. Rev. B 44 (1991) 12054.